Received: 27 March 2020 | Revised: 17 August 2020 | Accepted: 4 September 2020

DOI: 10.1002/nag.3145

WILEY

RESEARCH ARTICLE

An efficient transient-state algorithm for evaluation of leakage through defective cutoff walls

Yutao Pan[1] | **Michael A. Hicks**[2] | **Wout Broere**[2]

[1] Department of Civil and Environmental Engineering, Norwegian University of Science and Technology, Trondheim, Norway

[2] Faculty of Civil Engineering and Geosciences, Delft University of Technology, CN, Delft, the Netherlands

Correspondence
Yutao Pan, Department of Civil and Environmental Engineering, Norwegian University of Science and Technology, Høgskoleringen 7a, Trondheim 7491, Norway.
Email: yutao.pan@ntnu.no

Funding information
NRF-NSFC 3rd Joint Research Grant (Earth Science), Grant/Award Number: 41861144022

Abstract

Artificial barriers are widely used to prevent leakages. However, due to construction errors during the wall installation, passages with small dimensions may occasionally penetrate through the barrier, undermining its tightness. A three-dimensional discretized algorithm (TDA) is proposed for quantitatively estimating the transient-state discharge rate through defective cutoff walls. By discretizing the wall into a three-dimensional refined mesh grid, the algorithm enables an examination of penetrating passages, an evaluation of defect dimensions, and an estimation of discharge rate through the penetrating passages. A rigorous realization-by-realization comparison between the TDA and the finite element method (FEM) was made, and it was found that the TDA results show strong correlations with the FEM results, but at a remarkably lower ($1/10^3$-$1/10^4$) computational cost. The TDA generally gives a discharge rate that is 0.1-1.0 times greater than its FEM counterpart, as the lengthened seepage distance due to random corrugations in the penetrating untreated zone cannot be replicated by the TDA.

KEYWORDS
construction error, cutoff wall, groundwater, leakage, statistics

1 | INTRODUCTION

Underground cutoff walls are widely used in various applications to hinder groundwater flow, contaminant transport, and possibly heat conduction.[1–9] Depending on the intended function, site conditions, and budget, cutoff walls are constructed by many different approaches. In cases where heavy machinery can be readily deployed, diaphragm walls, slurry walls, sheet-pile walls, or secant-pile walls are usually used.[7,10–14] Conversely, in scenarios where the site conditions cannot support heavy machinery due to weak ground or limited clearance, such as islands or densely populated downtown areas, jet-grouting is a good option.[1,3,15–17]

Although cutoff walls are installed with due discretion (Figure 1A-D), leakages of groundwater[18–27] and contaminant in the form of leachate[2,6,28] have been widely observed in many parts of the world. Occasional construction errors were found to be one of the primary reasons for the leakages.[3,23,29]

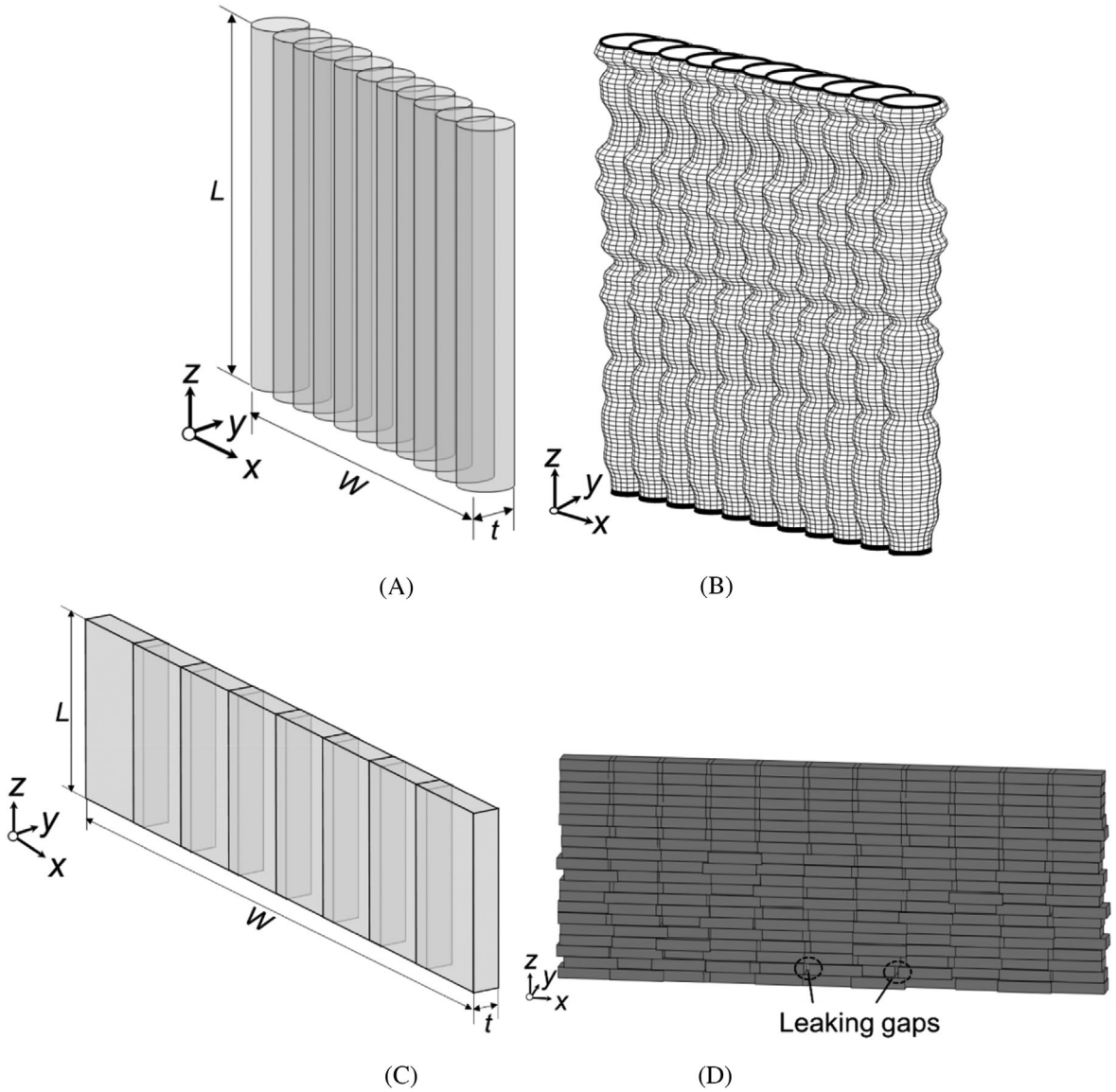

FIGURE 1 Two types of cutoff wall: (A) jet-grouted cutoff wall (ideal); (B) jet-grouted cutoff wall (defective); (C) diaphragm wall (ideal); and (D) diaphragm wall (defective)

In cases where small penetrating leakage passages occur, the performance of the barrier may be significantly undermined, leading to hidden leakages[5] or even catastrophic failures.[29,30] One option to evaluate the impact of geometric imperfection on the cutoff performance of the barrier is the random finite element method (RFEM), which can readily replicate the random heterogeneity of the permeability coefficient.[31–35] However, compared to the large dimensions of cutoff structures (10^1-10^3 m), the imperfections are usually tiny in size (10^{-2}-10^{-1} m). For example, a typical cutoff wall of an excavation project may be 20 m × 20 m × 1 m in the longitudinal, vertical, and transverse directions, respectively. Therefore, approximately 6.25 million constant-strain brick elements would need to be used to simulate the wall and replicate the small penetrating holes with a dimension of about 0.04 m in the numerical model. This would require a RAM of approximately 50 GB and 10^3 h to run a simple transient flow analysis on a single core with a central processing unit clock speed of 3.4 GHz. This makes it extremely difficult to implement RFEM on an ordinary workstation when thousands of Monte Carlo simulations are involved. In cases where instant onsite evaluation of the cutoff performance is required with existing inclination data, one cannot run a time-consuming finite element analysis to guide the ongoing construction. Hence, it is of engineering interest to develop an algorithm enabling a fairly accurate and speedy evaluation of the impact of geometric imperfections on the performance of the cutoff walls.

Van Esch et al[36] used Monte-Carlo simulations combining steady-state flow and geometric models of a jet-grout sealing layer composed of constant diameter columns with variable orientation and positioning of the jet-grout lance at the surface. They focused on the impact of the resulting variation in the relative positions of successively installed columns on the amount and size of imperfections, mainly caused by the overlap of successive columns and shadowing effects resulting in untreated soil volume, effects earlier signaled by Van Tol et al,[37] but they did not consider the impact of local variations in column diameter. Wu et al[38,39] investigated transient-state leakage through cutoff walls and segmental tunnel linings using large-scale, three-dimensional, coupled consolidation analysis. The defects were simulated as one-dimensional user-defined leakage elements to replicate the migration of water from the upstream side to the downstream side. However, in these studies, the size of the defects was assumed and the relationship between random construction errors and defects was not considered.

Pan et al[16,17,40] proposed a three-dimensional discretized algorithm (TDA) to evaluate the steady-state discharge rate of groundwater leakage through geometrically imperfect water barriers (eg, jet-grouted earth-plug, cutoff wall, and diaphragm wall). This algorithm was found to be reasonably accurate compared to RFEM (10-30% relative error), for calculation durations of only $1/10^3$-$1/10^2$ times those for RFEM. However, this algorithm is only applicable to steady-state problems, whereas time-dependent behavior is of significant engineering interest in many applications, such as in the evaluation of the breakthrough time of leachate through a cutoff wall in a landfill project[4,14,15,41] and the leakage detection of a cutoff wall in a deep excavation.[20,22,23] In such cases, a transient-state analysis is more relevant than a steady-state analysis.

The aim of this study is to develop a discretized algorithm to evaluate the transient-state discharge rate through geometrically imperfect cutoff structures installed against groundwater seepage, contaminant transport, and possibly heat conduction. Despite the vast difference in the physical backgrounds of the three applications, they share the same mathematical formulation, that is, Laplace's diffusion equation. The approach is first described in detail. Then, a preliminary validation with simple boundary conditions is conducted for a deterministic scenario. This is followed by a rigorous realization-by-realization validation in a random scenario. The results show that the proposed method can give a reasonably accurate estimation of the time-dependent discharge rate through a geometrically imperfect cutoff wall at a significantly lower calculation expense.

2 | METHODOLOGY

2.1 | Problem description

Cutoff walls are built with materials that have a significantly lower diffusion coefficient than the in-situ soils, creating a protective layer to prevent the exchange of flows (groundwater, contaminant, or heat) between two spaces. There are many types of construction error contributing to the geometric imperfections of cutoff walls, depending on the construction approach and workmanship. Typical construction errors include the inclination of the installation machines,[27,42,43] the variation of member dimensions,[3,43] and occasional soil inclusions.[27,42] For diaphragm walls, occasional soil inclusions, the particular shape of joints, gapping due to misalignment, and the inclinations of grabs are contributing factors to possible leakage.[27,42] For sheet pile walls, the inclination of the pile axis and the particular shape of joints are major factors.[9,44] Since the primary concerns in this study are the accuracy and calculation expense of the proposed algorithm, the seepage discharge (flow rate) through a jet-grouted cutoff wall is used as an example.

Jet-grouted cutoff walls generally suffer from two origins of construction error, that is, the random inclination of the column axis and the random variation of the diameter along the column axis.[3,41] The random inclinations lead to the decoupling of adjacent jet-grouted column members, and this effect becomes worse with increasing depth. It can be described by two angles,[16,17,45–49] that is, the azimuth (α) and the inclination angle (β), Figure 2A, which can be simulated using random variables. Moreover, the column diameter has been simulated as a one-dimensional random process.[16,17] The scale of fluctuation (SOF) of the column diameter was set equal to the vertical SOF of the soil, because the diametric variation was assumed to be mainly attributed to the soil profile's stratified structure.[50–52] A possible variation in the origin of each column at the surface is not taken into account in this study, as jet-grouted walls are mostly composed of a single line of columns and the resulting geometric imperfections are more relevant for the jet-grouted base layers.[37] The statistical characteristics of the axis inclination parameters and the column diameter are summarized in Table 1.

In this section, a three-dimensional model is first established to capture and evaluate the geometrical imperfections. Then, an evaluation approach for discharge rate through the defective cutoff wall is proposed. The flowchart of the TDA

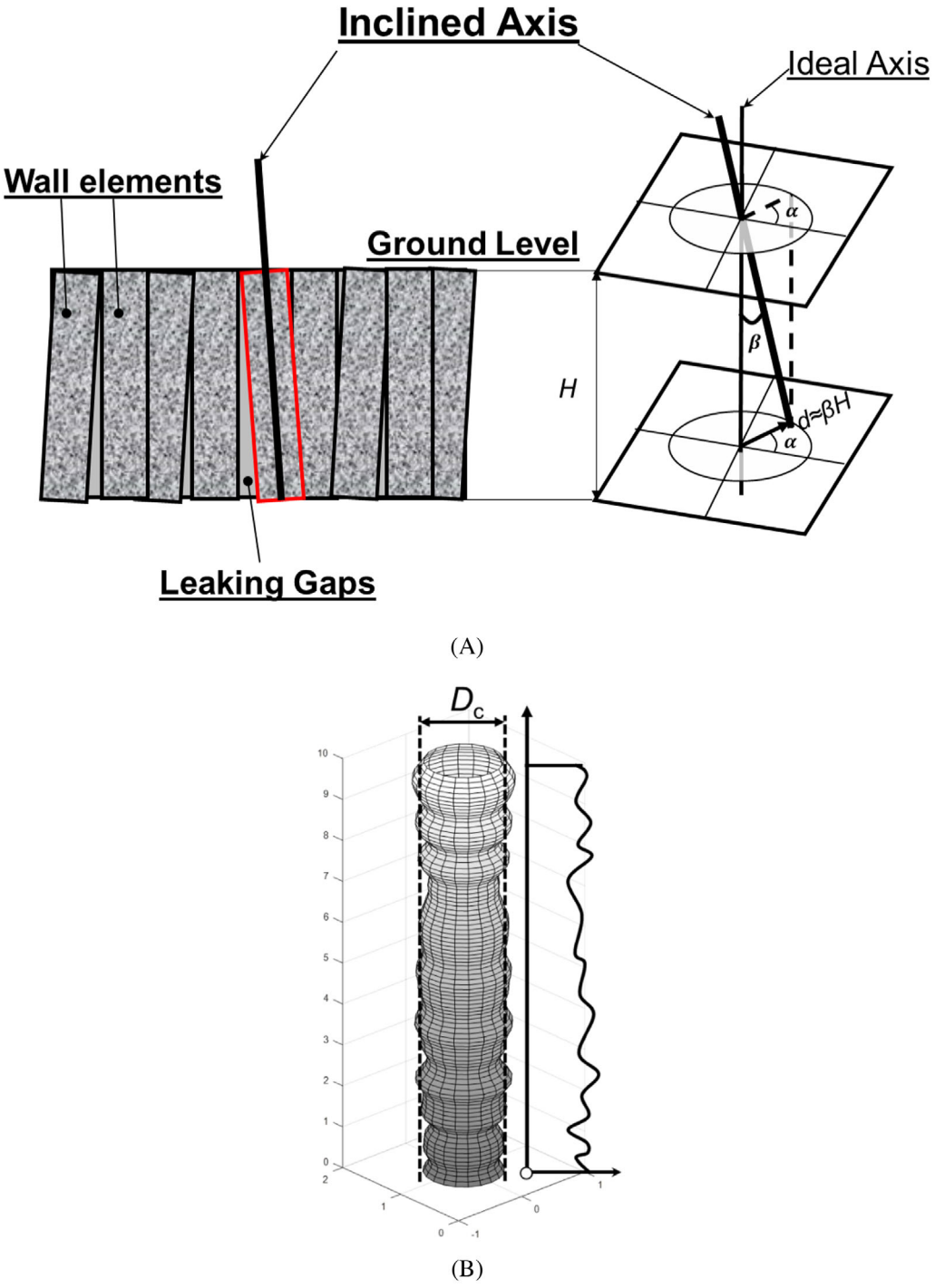

FIGURE 2 Illustration of geometric imperfections: (A) random inclinations; and (B) random diametric variation

is shown in Figure 3A. The main idea of the TDA is to find all the penetrating passages and then simplify them as one-dimensional channels with spatially varying cross-sectional areas. By doing so, one only needs to calculate the discharge rate through each penetrating passage and then sum up the contributions from all channels.

2.2 | Quantification of geometric imperfections

Following Pan et al,[16,17] the ground domain is first discretized into identical eight-node cuboids, creating an equally spaced lattice of nodes, Figure 4A and B. The vertical planes (parallel to the *x*-*z* plane) are called slices. The coordinates of each

TABLE 1 Variability of geometric imperfection of jet-grout column

No.	Type of natural soil	Average diameter (m)	COV(D_c)*	S.D. (β)**	Remarks	Source
1	Clay-silt	-	0.02-0.05	-	-	Croce et al[58]
	Sand		0.02-0.10		-	
	Gravel		0.05-0.25		-	
2	Sandy clay	1.1	0.06-0.19	-	Derived from field data of diameter at different depths, horizontal column	Langhorst et al[59]
3	Silty sand	0.71-1.11	0.06	0.07°***	Vertical columns at Vesuvius site	Croce and Modoni[3]
	Sandy gravel	1.06-1.20	0.19		Vertical columns at Polcevera site	
4	Silty sand	2.5	-	0.16°	Vertical columns at Barcelona site	Eramo et al[60]
5	Sandy clay	0.38	0.13	-	Vertical column with lower water content	Arroyo et al[46]
		0.48		-	Vertical column with lower water content	
		0.75	0.17	0.17°	(Sub) Horizontal column	

*COV(D_c) is the coefficient of variation of column diameter.
**S.D. (β) is the standard deviation of column inclination.
***This standard deviation of inclination was obtained from a different site (Isola Serafini).

node are examined to determine whether it falls within the zone of a treated column (Figure 4B). If a node is not part of a treated column, it is then marked as untreated, as highlighted by the solid points in Figure 4B.

A penetration examination is required, because the discharge rate would increase sharply if the untreated zones form continuous seepage passages (the permeability coefficient of granular untreated soil is about 100-1000 times that of the treated soil[53]). This can be done by scanning the succession of untreated zones along the possible seepage passage (y-direction). If untreated nodes exist in each slice, and there is a continuous overlapping of untreated zones for successive slices, the untreated zone is considered to penetrate the cutoff wall. Figure 4C shows three scenarios to illustrate the penetration examination. The first scenario shows no penetration because the highlighted slice is completely treated. Scenario 2 shows no penetration because the two highlighted slices have no overlap. Only scenario 3 shows penetration of the wall.

For a penetrating passage, the untreated cross-sectional area for each slice is evaluated by counting the number of untreated nodes, Figure 4B. Specifically, one node would represent an area that is equivalent to the area of the brick element's cross-section. When all the nodes are counted, the untreated cross-sectional areas in the seepage direction (y-direction) can be evaluated, Figure 4D.

2.3 | Estimation of discharge rate of penetrated cutoff walls

With the evaluated cross-sectional areas along the seepage passage, it is interesting to know the corresponding transient-state discharge rate. This section provides a quantitative evaluation method to bridge the gap between the size of the geometric imperfection and the discharge rate. In this study, the groundwater seepage through a defective cutoff wall is used as an example.

Previous studies[38,39] have shown that the transient-state discharge rate through defective cutoff walls is influenced by the properties of the defects and the ambient boundary conditions. The former includes the geometry, permeability coefficient, and constrained modulus of the untreated zones. The latter includes the groundwater conditions (groundwater supply and groundwater level), permeability coefficient, and constrained modulus of the surrounding soil. In this study, only the properties of the defects were considered. The effect of complex boundary conditions, though of practical engineering interest, is beyond the scope of this study.

Pan et al[16,17,40] derived a theoretical solution for steady-state groundwater discharge rate through a geometrically imperfect water barrier. The discharge rate was found to be proportional to the harmonic average of the cross-sectional areas of the untreated zone along the seepage passage,

$$q = \frac{kH}{T_{wall}} \tilde{A}\left(T_{wall}\right), \tag{1}$$

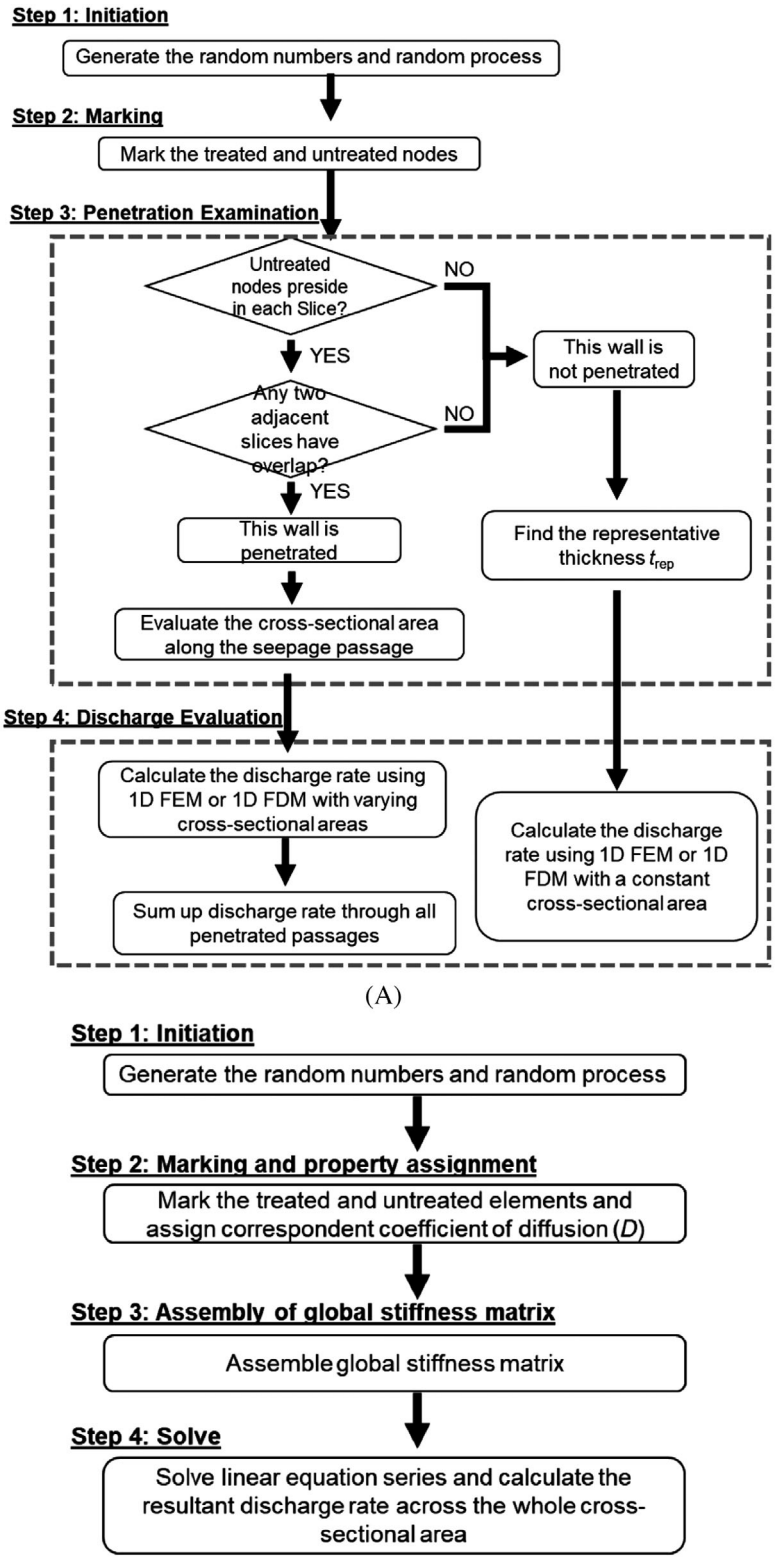

FIGURE 3 Illustrations of the algorithms: (A) flowchart of the TDA; and (B) pseudo code of the in-house three-dimensional FEM considering geometric imperfections (FEM3D)

where q is the resultant discharge rate through the defective cutoff wall, $\tilde{A}(T_{wall}) = \frac{1}{\frac{1}{T_{wall}}\int_0^{T_{wall}} \frac{1}{A(u)} du}$ is the harmonic average of the areas along the seepage passage, T_{wall} is the nominal thickness of the wall, k is the permeability coefficient of the untreated zones, and H is the head difference between the two sides of the wall. However, this approach was based on mass conservation, which implicitly assumes a steady-state scenario. The governing equation needs to be revisited to evaluate the transient-state discharge rate through the wall.

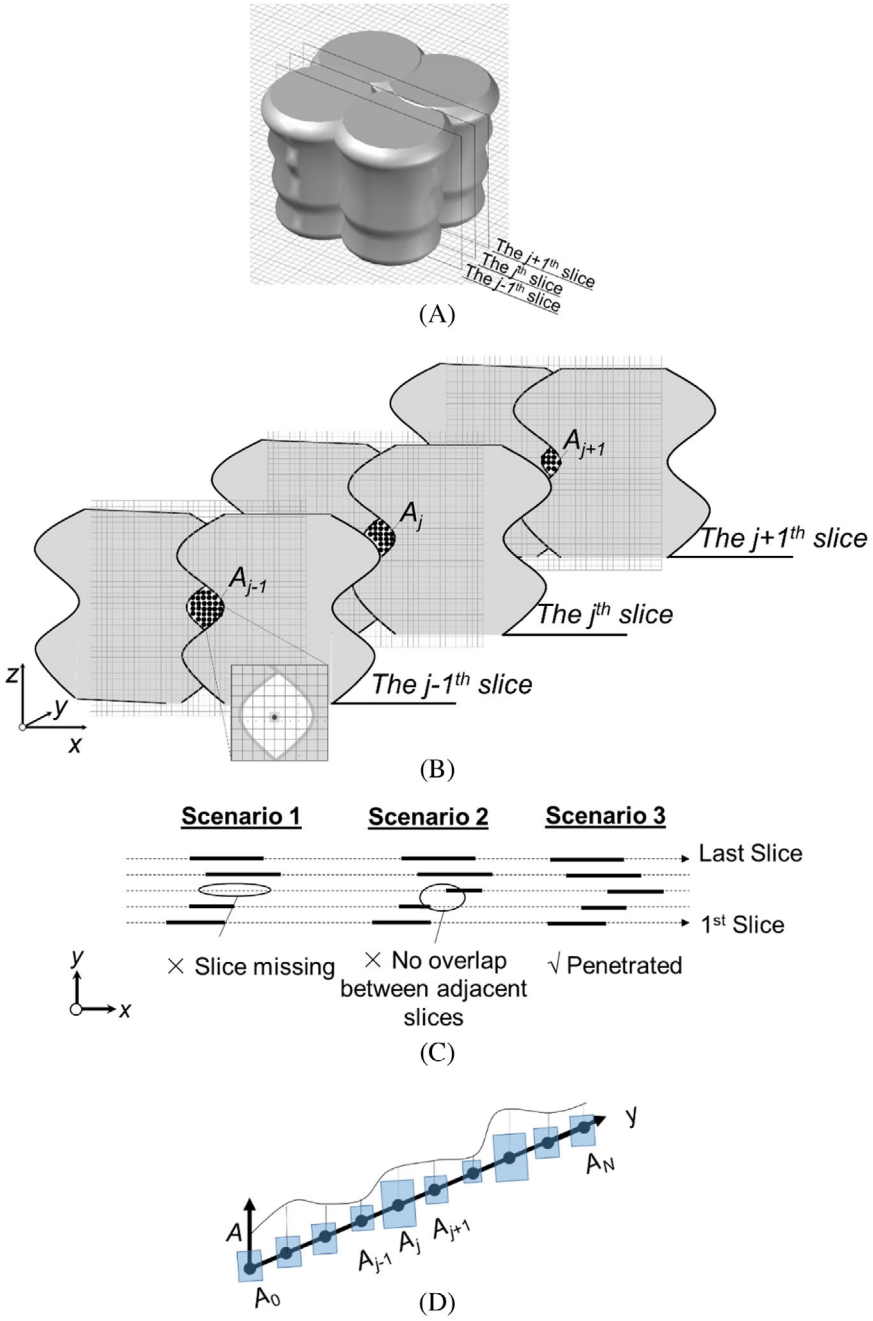

FIGURE 4 Illustration of discretization and evaluation of cutoff performance: (A) three-dimensional view; (B) evaluation of untreated cross-sectional area for each slice; (C) illustration of penetration examination (the thick solid line represents the location and size of the untreated slice); and (D) illustration of untreated cross-sectional area along a penetrating seepage passage

Figure 5 shows an infinitesimal segment of an untreated passage with spatially varying cross-sectional area. The general formulation of transient-state diffusion (Laplace's equation) can be written as:

$$A\frac{\partial \phi}{\partial t} = \frac{\partial}{\partial y}\left(DA\frac{\partial \phi}{\partial y}\right), \tag{2}$$

where A is the cross-sectional area of the diffusion passage, which varies with the y-coordinate; ϕ is the potential, which, for seepage problems, represents the total water head; and D is the coefficient of diffusivity, which is here regarded as a constant, even though there is spatial variability in this parameter. This simplification is not unreasonable since the difference in diffusion coefficient between treated and untreated soils is much more significant than the spatial variability within one material. In the case of seepage, D is essentially the coefficient of consolidation, which is related to the permeability coefficient, constrained modulus, and bulk unit weight, as shown in Table 2.

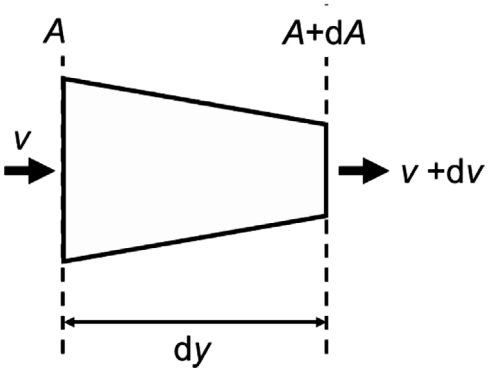

FIGURE 5 Infinitesimal segment of a one-dimensional flow problem with spatially varying cross-sectional area

TABLE 2 Meaning of variables in Laplace's equation for different engineering applications

Parameter	Symbol	Seepage	Heat transfer
State variable	ϕ	water head unit: m	Temperature unit: K
Coefficient of diffusivity (unit: m^2/s)	D	$D=\frac{k}{\gamma_w m_v}$ k- coefficient of permeability (unit: m/s); γ_w- unit weight of water (unit: kN/m^3); m_v- compressibility coefficient (unit: m^2/kN)	$D=\frac{k}{\rho c}$ k- thermal conductivity (unit: W/m/K); ρ- density (unit: kg/m^3); c- specific heat capacity (unit: J/kg/K)
Discharge rate	q	unit: m^3/s	unit: W

In this study, the cross-sectional area along the penetrating passage (A) is a continuous random process and cannot be represented by an elementary function. Hence, Equation (2) has no explicit solution, although numerical approaches, such as the finite difference method, can be used to solve the equation.

Since the cross-sectional area A varies with the y-coordinate, it cannot be cancelled out from both sides of the equation. Hence, Equation (2) can be written as:

$$\frac{A}{D}\frac{\partial \phi}{\partial t} = \frac{\partial A}{\partial y}\frac{\partial \phi}{\partial y} + A\frac{\partial^2 \phi}{\partial y^2}. \tag{3}$$

The spatial and temporal spaces are discretized to facilitate the implementation of the finite difference method, Figure 6. The number of spatial intervals is set equal to the number of slices shown in Figure 4D. Using a forward difference in time for $\frac{\partial \phi}{\partial t}$ and a central difference for spatial derivatives (cross-sectional area A and potential value ϕ), Equation (3) can be rewritten as:

$$\frac{A_j}{D}\frac{\phi_j^{m+1}-\phi_j^m}{\Delta t} = \frac{A_{j+1}-A_{j-1}}{2\Delta y}\frac{\phi_{j+1}^m-\phi_{j-1}^m}{2\Delta y} + A_j\frac{\phi_{j+1}^m-2\phi_j^m+\phi_{j-1}^m}{\Delta y^2}, \tag{4}$$

FIGURE 6 Illustration for the one-dimensional finite difference method with spatially variable cross-sectional area

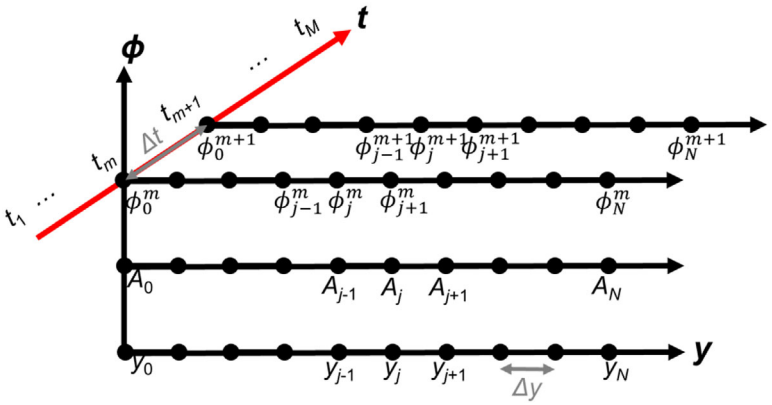

where ϕ_j^m is the potential value at the jth slice and mth time node; Δy is the spatial interval,$\Delta y = \frac{T_{Wall}}{N}$; N is the number of spatial intervals in the y-direction (so that the number of spatial nodes is N+1); Δt is the time interval, $\Delta t = \frac{T}{M}$; T is the total time duration of the transient flow; and M is the number of time intervals (so that the number of time nodes is M+1).

Reformulating Equation (4) gives:

$$\phi_j^{m+1} = \phi_j^m + \frac{D\Delta t}{\Delta y^2}\left(\frac{A_{j-1} + 4A_j - A_{j+1}}{4A_j}\phi_{j-1}^m - 2\phi_j^m + \frac{-A_{j-1} + 4A_j + A_{j+1}}{4A_j}\phi_{j+1}^m\right). \tag{5}$$

At time $t = t_m$, there are $(N + 1)$ unknowns and $(N-1)$ equations of the form of Equation (5). Since the potential values on either side of the wall are assumed constant, the Dirichlet boundary conditions are used:

$$\begin{Bmatrix} \phi_0^m = H \\ \qquad (m = 1, 2, \ldots, M) \\ \phi_N^m = 0 \end{Bmatrix}. \tag{6}$$

At the initial state (t=0), only the upstream side has a potential value of H, while all other nodes have a zero potential value,

$$\begin{Bmatrix} \phi_0^0 = H \\ \phi_j^0 = 0 \; (j = 1, 2, \ldots, N) \end{Bmatrix}. \tag{7}$$

The potential value (ϕ_j^m) at each node ($j = 0, 1,\ldots, N$) at time t_m can be calculated by solving the linear equation series with $(N + 1)$ unknowns and $(N + 1)$ equations. Both the grid size and the time step play a crucial role in the stability, convergence, and accuracy of the finite difference method.[54] The discharge rate at each node ($j = 0, 1,\ldots, N$) at time t_m can be evaluated using:

$$q_j^m = k\frac{\phi_{j+1}^m - \phi_{j-1}^m}{2\Delta y}A_j, \tag{8}$$

where k is the coefficient of conductivity. Following Pan et al,[16,17] in cases where there are multiple penetrating seepage passages, the one-dimensional transient discharge rate along each seepage passage is calculated separately. The resultant discharge rate of the whole cutoff wall is then the summation of all seepage passages.

Alternatively, the one-dimensional flow can also be simulated using a standard one-dimensional finite element method (FEM). In this study, the FEM approach was revised from Schirén's[55] approach, which was developed to simulate one-dimensional heat diffusion with linear elements. Since diffusion problems share the same governing equation (Equation 2) as the seepage problem, the same approach can be used. To do so, the thermal conductivity is substituted by the coefficient of permeability, while the product of density and specific heat capacity is substituted by the product of unit weight of water and compressibility coefficient. The respective meanings of the parameters in each application scenario are summarized in Table 2.

A bar element with two nodes was used, with each node having one degree of freedom; that is, total head. Two parameters were defined for each element; that is, coefficient of diffusivity (D) and cross-sectional area (A). The coefficient of diffusivity was assumed to be constant, as mentioned above, whereas the cross-sectional area varies along the penetrating passage. One element was assigned for each slice shown in Figure 4D, with the cross-sectional area associated with each element equaling the cross-sectional area evaluated in the TDA algorithm. The one-dimensional FDM and FEM approaches were separately incorporated in the TDA, and comparisons were made as will be shown later on.

Equation (2) may also be used to describe contaminant diffusion (or advection) and heat conduction problems. However, the contaminant transport problem is more complicated as it consists of advection, diffusion, and dispersion, and, although the advection and diffusion both follow Equation (2), they have different boundary conditions. The former stems from the transport of a substance by bulk motion, namely, the groundwater seepage. It is highly dependent on the hydraulic boundary conditions, that is, water head difference. In contrast, the latter describes the spread of concentration and is only related to the concentration boundary. There are many scenarios where either advection or diffusion is predominant. For example, in landfills where a high water head difference occurs between either side of the cutoff wall, advection

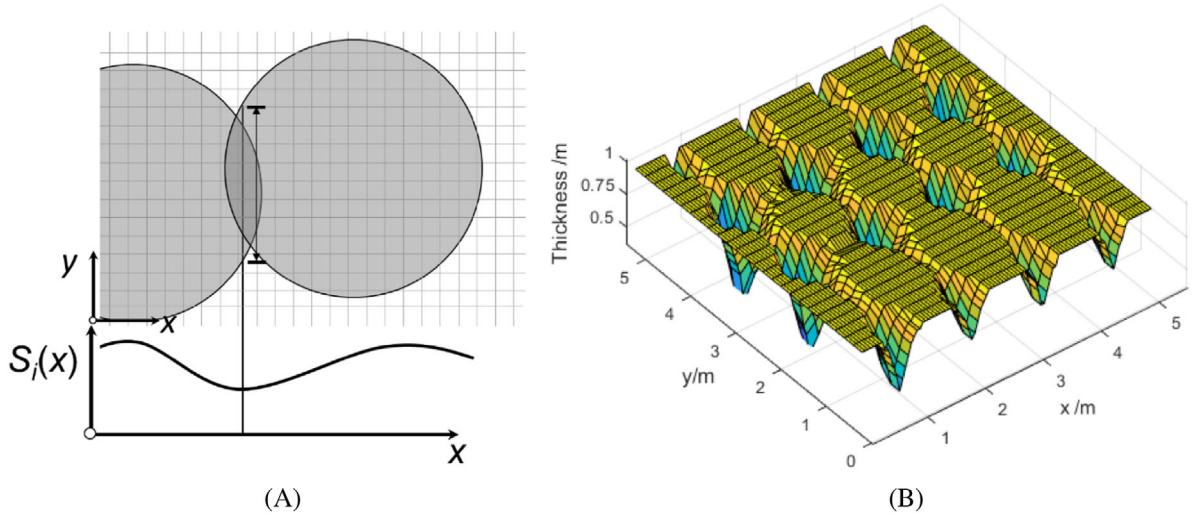

FIGURE 7 Illustrations of wall thickness: (A) evaluation of wall thickness; and (B) typical realization of wall thickness

may dominate. In a recent landfill project in Suzhou,[6] the head difference was about 10 m, indicating the dominance of advection. In cases where the water head difference is negligible and the seepage velocity is very low, diffusion prevails. In cases where the advection and diffusion are both significant, a one-dimensional FEM code for coupled advection-diffusion may be incorporated into the TDA. However, detailed verifications of such a case merit extensive study and are beyond the scope of this paper.

2.4 | Estimation of a representative thickness

When the cutoff wall is not penetrated by untreated zones, the discharge rate is much lower than for the penetrated cases, as will be shown later. In unpenetrated cases, a representative thickness should be used to characterize the water-tightness, following Croce and Modoni[3] and Pan et al.[40] The thickness of the wall can be evaluated by counting the number of treated nodes in the *y*-direction, as shown in Figure 7A. A typical realization of wall thickness distribution is plotted in Figure 7B. In Pan et al,[40] the minimum thickness was used as the representative thickness because it is on the conservative side. The applicability of the minimum thickness in the transient state will be examined later.

3 | COMPARISON WITH FEM

The FEM is one of the most widely used approaches to investigate diffusion problems. The method proposed in this study is validated by FEM for both deterministic and random scenarios. Although commercial software, such as Plaxis, Geostudio, and Abaqus, can readily simulate the deterministic flow problem, there are some technical difficulties that hinder their implementation in random scenarios in which the random material properties depend on element coordinates.[17] The most pronounced problem is that these finite element programs do not allow one to assign the permeability coefficients at the element level. Instead, they only allow permeability to be assigned at the block level. This eliminates the possibility of assigning permeability coefficient using the user-defined material interface provided by Plaxis or Abaqus. Hence, an in-house three-dimensional FEM program for transient flow problems was coded in Matlab (referred to as FEM3D), this being an upgraded version of the steady-state code in Pan et al.[40] The pseudo code of FEM3D considering geometric imperfections is summarized in Figure 3B. A preliminary verification study for transient-state flow through a homogeneous unit block showed that the three-dimensional FEM code gives the same result as the commercial software Geostudio.

In this section, the seepage through a jet-grouted cutoff wall was used as an example to verify the TDA in both deterministic and random scenarios. For the deterministic scenario, the results of the TDA approach were checked against the results of both FEM3D and the commercial FEM software Geostudio. For the random scenario, a rigorous realization-by-realization comparison between the TDA and FEM3D was conducted.

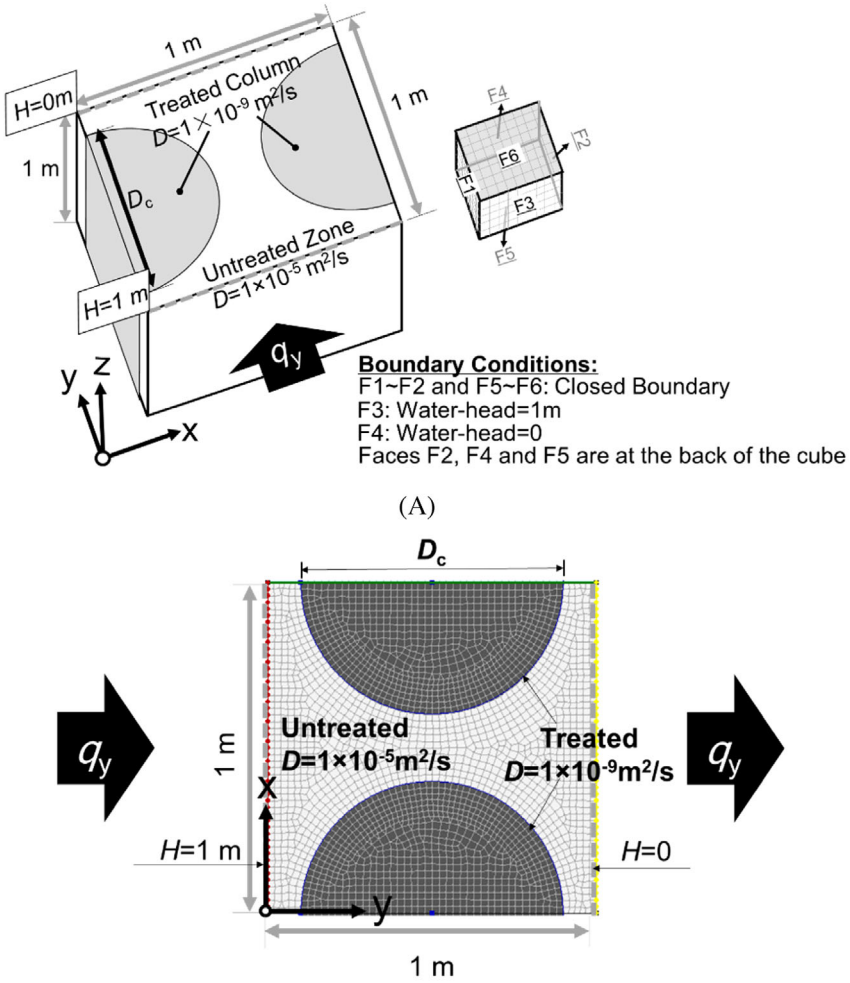

FIGURE 8 Simple verification model for deterministic scenario: (A) boundary conditions and numbering of the six faces (indicated by F1-F6); (B) boundary conditions and mesh for FEM model using Seep/W (number of elements = 2600; element type is linear-strain quadrilateral or triangular element)

Although a case study with field data is desirable, there are currently no valid data for discharge rate through a defective cutoff wall. This is mainly because the leakage discharge rate underground is difficult to measure. Although field data of ground settlement and groundwater level are available,[22] they do not provide direct information on the resultant discharge rate.

3.1 | Deterministic scenario

Figure 8A shows that the model was a unit cube with a side length of 1 m. The front (F3) and back (F4) faces were assigned a total head of 1 and 0 m, respectively, whereas the other four boundaries were closed. This implies that the groundwater migrates from the front (upstream) face to the back (downstream) face. The two treated columns are not overlapping and thereby represent a discontinuous cutoff wall.

Figure 8B shows that two vertical columns with a diameter (D_c) were treated, while the other zones were untreated. This essentially makes the model a two-dimensional model. The diffusion coefficients of the treated and untreated zones were set as 1×10^{-9} and 1×10^{-5} m^2/s, respectively. Two thousand and five hundred identical cuboidal elements, with dimensions of 0.02 m × 0.02 m × 1.00 m in the *x*-, *y*-, and *z*-directions, were used. The mesh size in the *z*-direction was much larger because the problem was essentially two-dimensional. The resultant discharge rate in the three-dimensional FEM analysis was evaluated by summing up the *y*-direction local discharge rates in all elements on the face F4. The same mesh size was used for the TDA. The untreated cross-sectional area at each *y*-coordinate (Figure 9A upper subplot) was evaluated and then used to calculate the discharge rate by both the one-dimensional finite difference method (TDA-FDM) and the one-dimensional finite element method (TDA-FEM).

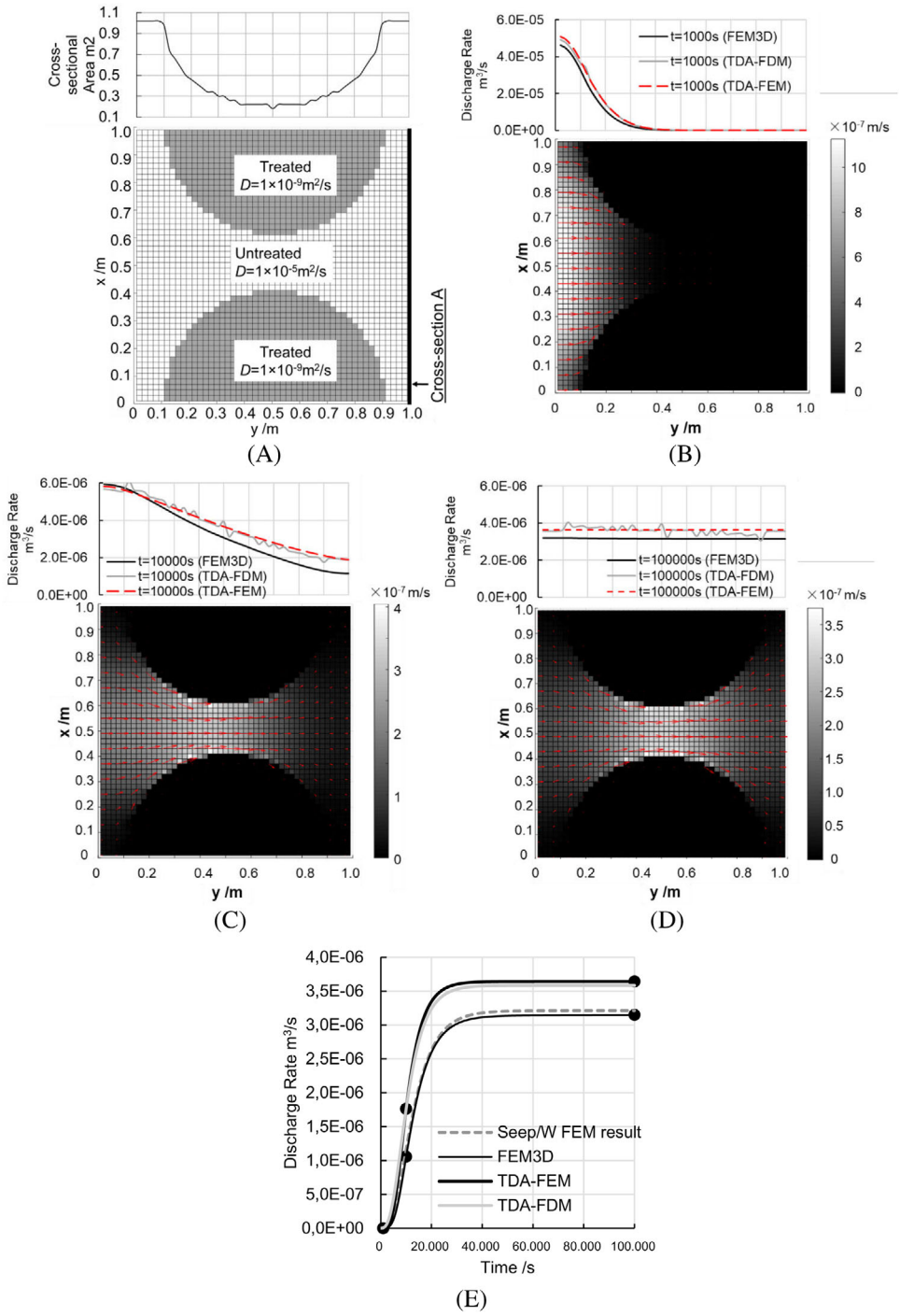

FIGURE 9 Comparison between FEM3D and TDA: (A) mesh (x-, y- element size = 0.02 m; z-element size = 1 m; number of elements = 2500; element type, 8-node brick element); (B) transient flow at t = 1000 s (upper subplot: resultant discharge rate at different cross-sections; lower subplot: flow velocity contours and vectors, unit: m/s); (C) transient flow at t = 10 000 s; (D) transient flow at t = 100 000 s; and (E) resultant discharge rate at cross-section A with time

Figure 9B lower subplot shows the contours and vectors of flow velocity from FEM3D at 1000 s. As expected, the seepage only reaches around one-third of the total thickness of the model, indicating the initiation of seepage at this moment. The resultant discharge rates for cross-sections with different y-coordinates were calculated by numerically integrating the flow velocity over the x-coordinate. On the other hand, the discharge rate at each y-coordinate was also calculated using the TDA via Equation (8). Figure 9B upper subplot shows that the TDA results match the FEM result reasonably well. Some numerical fluctuations can be observed in the resultant discharge rate versus y-coordinate curves in the TDA-FDM

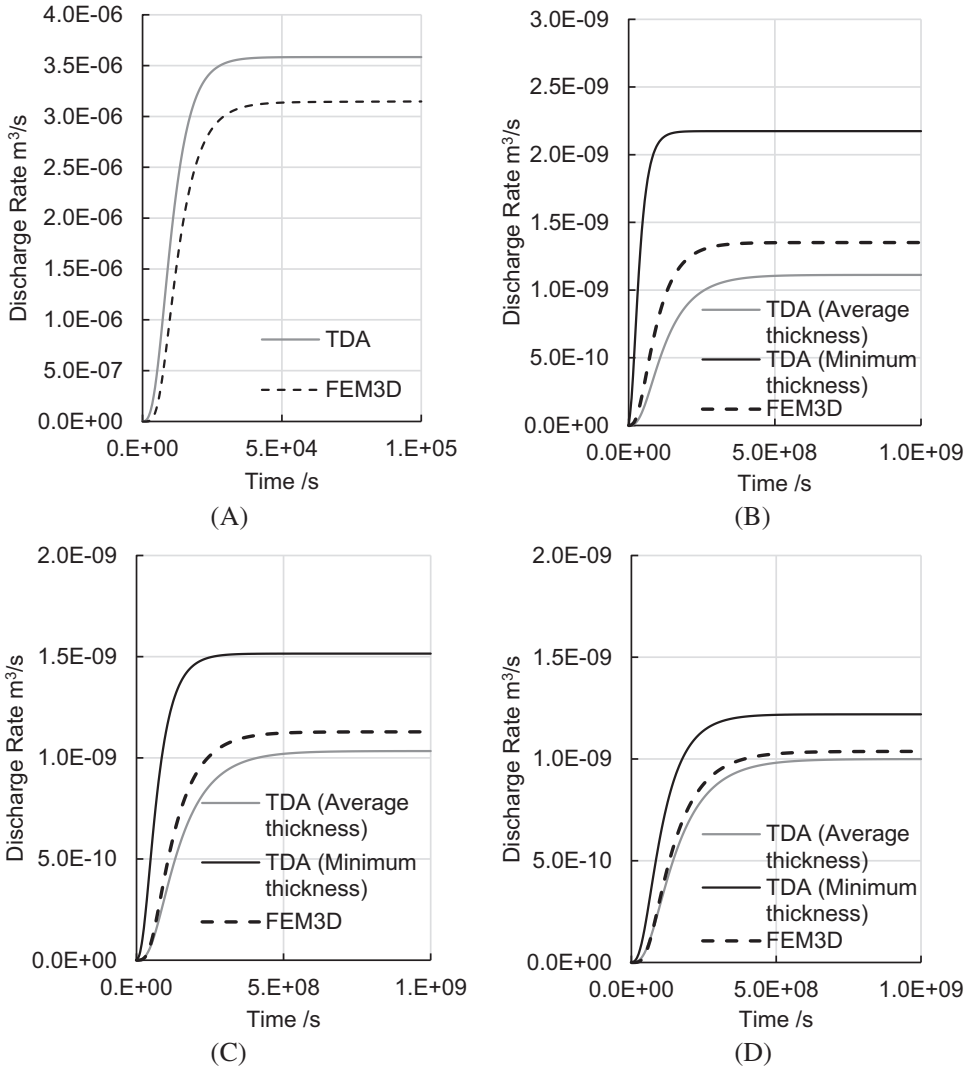

FIGURE 10 Verification in deterministic cases with columnar treated member: (A) comparison of resultant discharge rate at the downstream cross-section for column radius of 0.4 m; (B) comparison of resultant discharge rate at the downstream cross-section for column radius of 0.55 m; (C) comparison of resultant discharge rate at the downstream cross-section for column radius of 0.6 m; and (D) comparison of resultant discharge rate at the downstream cross-section for column radius of 0.65 m

results, especially at larger times. This is because the cross-sectional area was not strictly differentiable due to the use of discretization, as inferred from the upper subplot of Figure 9A. In contrast, the TDA-FEM results are smoother. By 10 000 s, the seepage has reached the end of the model, $y = 1$ m, Figure 9C. The TDA result is slightly higher than the FEM3D result. By 100 000 s, the seepage reaches the steady-state condition, with the discharge rate in the seepage direction being almost constant, Figure 9D. At this moment, the TDA result is higher than the FEM3D result, which is consistent with Pan et al.[40] Figure 9E shows the evolution of the resultant discharge rate at $y = 1$ m. This location is crucial because it represents the downstream side of the cutoff wall. The discharge rate using the TDA is consistently higher than that computed using FEM3D over time. On the other hand, the FEM3D result slightly lags behind the TDA solution. This is ascribed to the one-dimensional assumption of the TDA, which ignores the elongation of the flow path in a two-dimensional case. The elongation of the flow path in the FEM3D analysis would potentially reduce the discharge rate and postpone its build-up. To further validate the model, the same problem was simulated using Geostudio (Seep/W 2D), using the two-dimensional mesh and boundary conditions shown in Figure 8B. The resultant discharge rate over time closely matched the FEM3D solution, indicating the validity of the FEM3D code. Given that the TDA-FEM result is smoother than the TDA-FDM result, only the TDA-FEM result is used hereafter.

For cases with a column radius of 0.4 m (Figure 10A), the untreated zone penetrates the cutoff wall, and the FEM3D result for the discharge rate is lower and slightly lags behind the TDA counterpart. For cases with a larger column radius

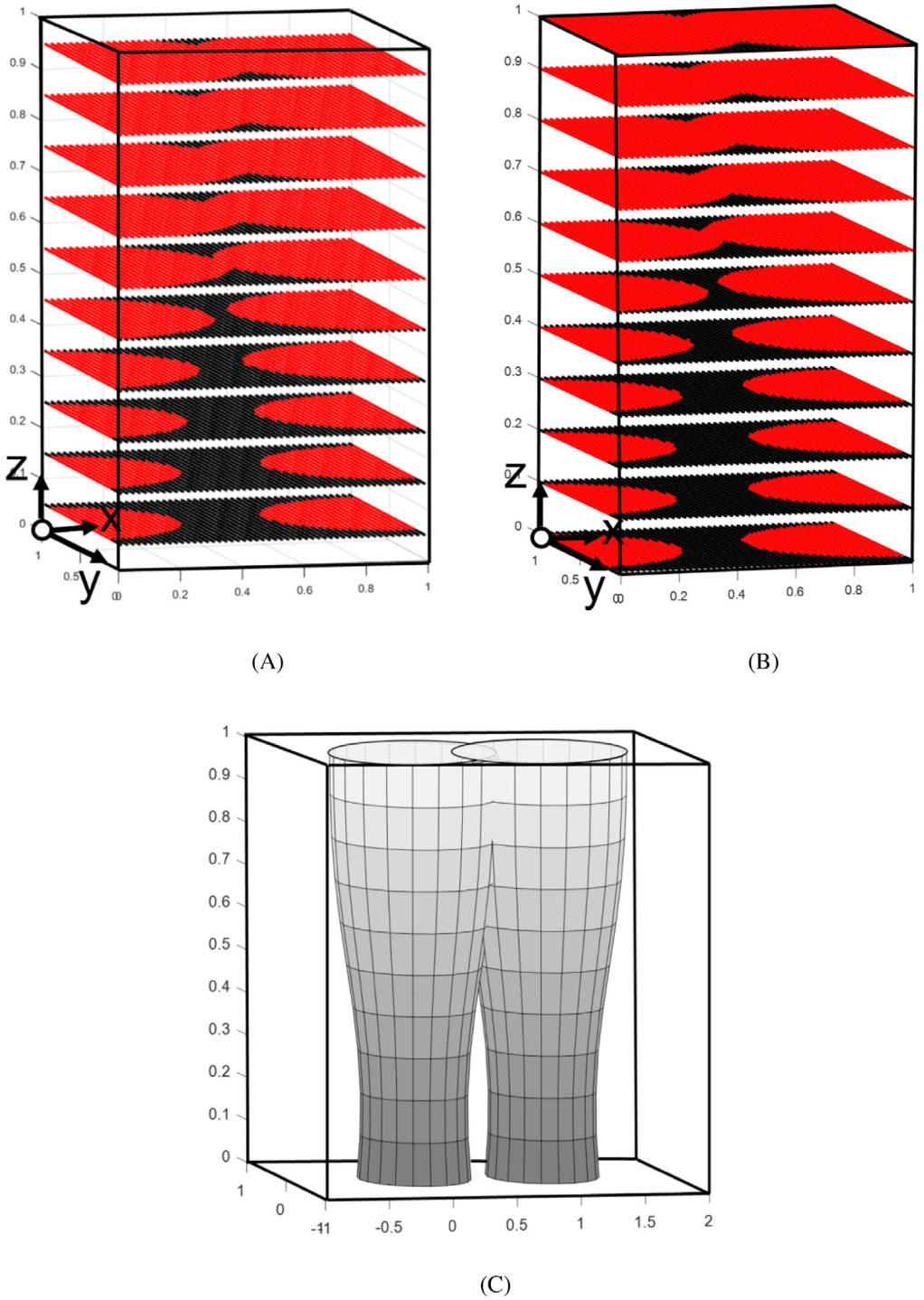

FIGURE 11 Treated and untreated zones in a random realization: (A) FEM (the red and black dots represent the centers of treated and untreated elements, respectively); (B) TDA (the red and black dots represent the treated and untreated nodes, respectively); (C) three-dimensional view of the unit cell (the two columns are fully plotted to facilitate viewing of the column shape, although the unit cell only consists of one half of each column)

(0.55, 0.6, and 0.65 m), the cutoff wall is not penetrated by an untreated zone. Hence, the wall is treated as a homogeneous block with a representative thickness, using Equation (8). Following Croce and Modoni[3] and Pan et al,[17] the minimum thickness is first used as the representative thickness. Figures 10B-D show that the TDA result calculated using the minimum thickness is consistently higher than the FEM3D result and reaches the steady-state earlier than the FEM3D counterpart, indicating that this approach is much more conservative than the FEM3D result. The TDA results calculated using the average thickness look more consistent with FEM3D in terms of the discharge rate and time of reaching the

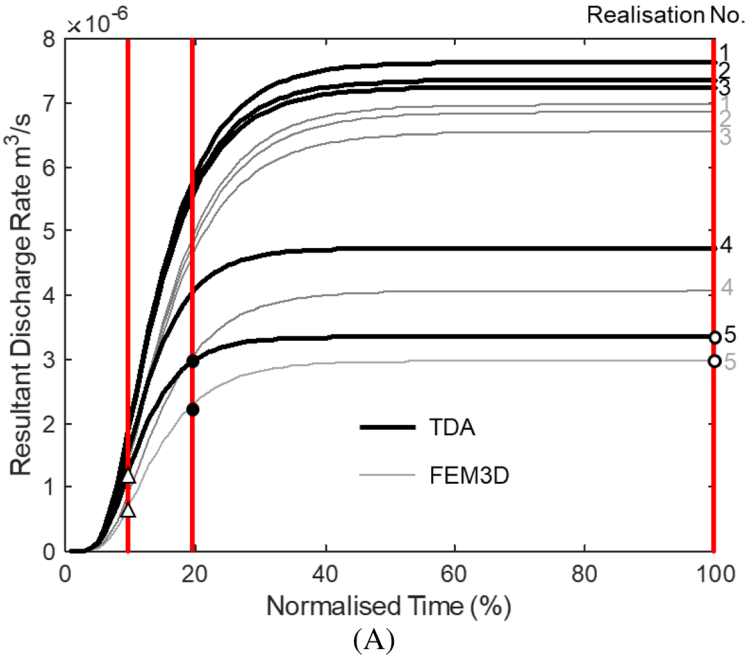

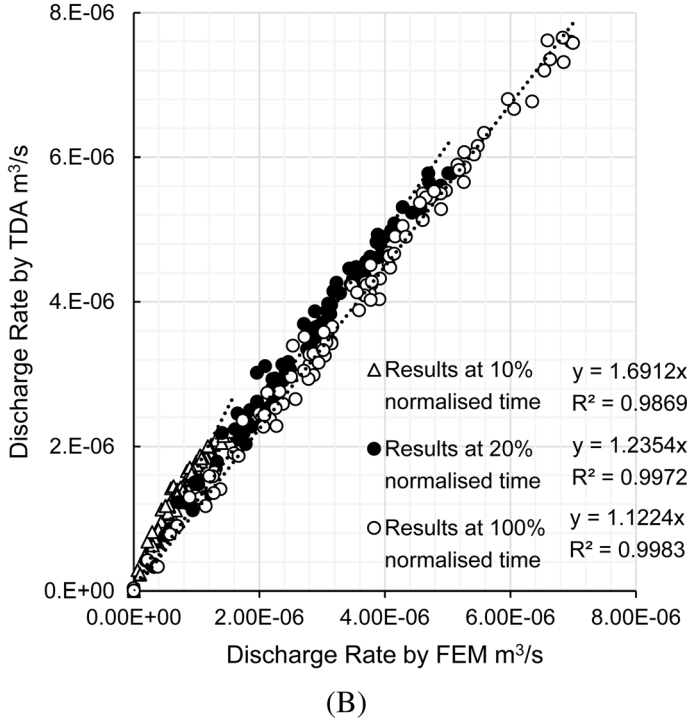

FIGURE 12 Verification in random cases with columnar treated member (Case VR1 in Table 3: average column diameter = 0.8 m): (A) transient-state discharge rate curves versus normalized time (only five realizations are plotted to distinguish the TDA and FEM realizations); (B) realization-by-realization comparison of discharge rate at three normalized times

steady-state, although they are slightly less conservative than the FEM3D results in terms of steady-state discharge rate. Hence, the average thickness was used as the representative thickness in the unpenetrated cases.

3.2 | Random scenario

In the random scenario, the column diameter varies along the column axis, and the column axis tilts randomly. The column diameter was simulated using a one-dimensional random process with a marginal normal distribution with a COV of 0.2 and an SOF of 1 m, following Pan et al.[16,17] The mean diameter depends on the jet-grouting parameters (such as the grouting pressure) and the soil profile. The random inclination parameters (α and β) were simulated using independent and identically distributed (i.i.d.) variables. This is because single-shaft jet-grouting rigs are usually relocated and recal-

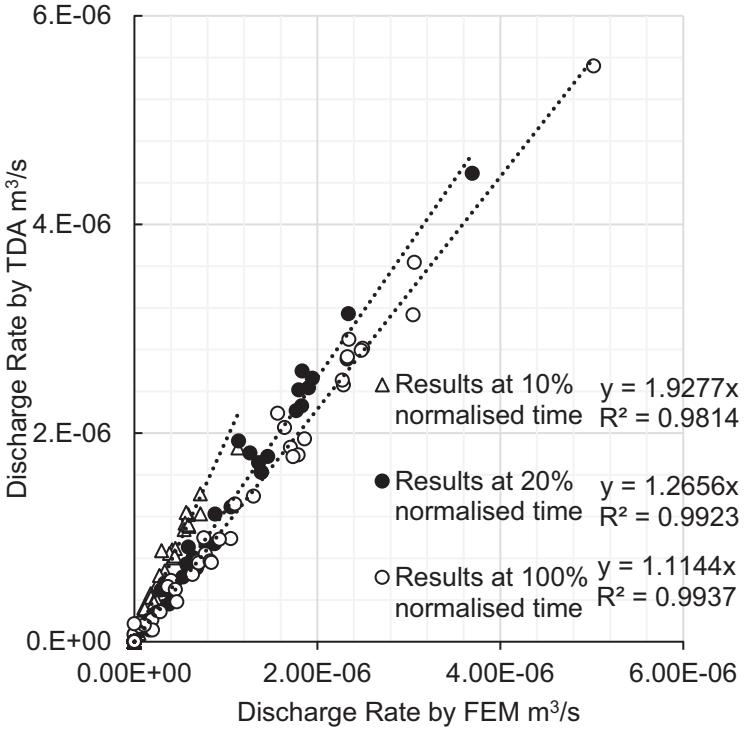

(A)

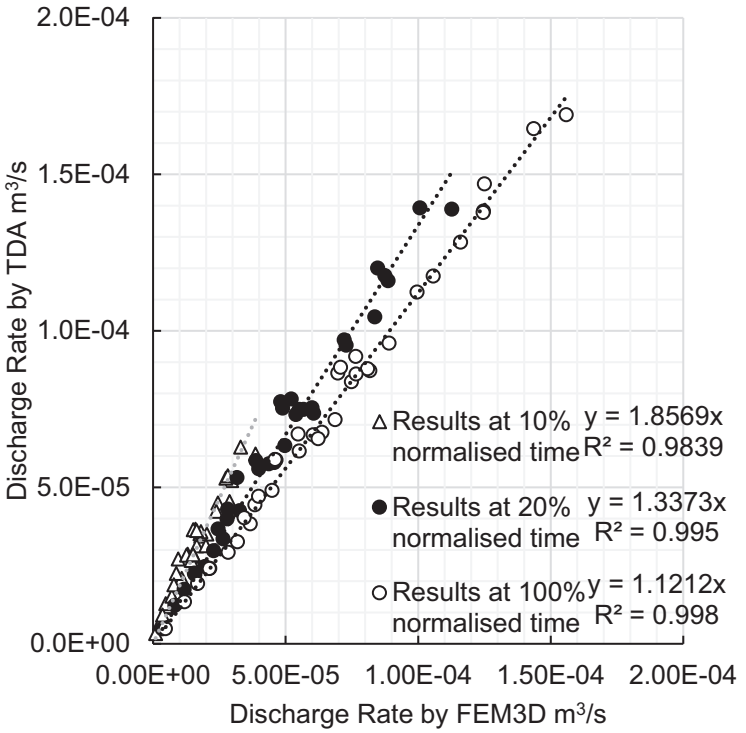

(B)

FIGURE 13 Verification in random cases with columnar treated member: (A) realization-by-realization comparison of discharge rate at three timings (Case VR2 in Table 3: average column diameter = 1.2 m); and (B) realization-by-realization comparison of discharge rate at three timings (Case VR3 in Table 3: model scale 9 m × 1 m × 10 m)

ibrated after installing one column. For multishaft rigs, however, the random inclinations are correlated. In this study, only single-shaft jet-grouting is considered as an example. The azimuth (α) follows a uniform distribution within [0, 2π], as it can tilt in any direction. The inclination angle follows a normal distribution with a zero mean and a standard deviation of 0.3 degrees.[3] The same random seeds for generating the random process of the column diameter and the random inclination parameters (α and β) were used for both the TDA and FEM3D. This is to ensure that precisely the same real-

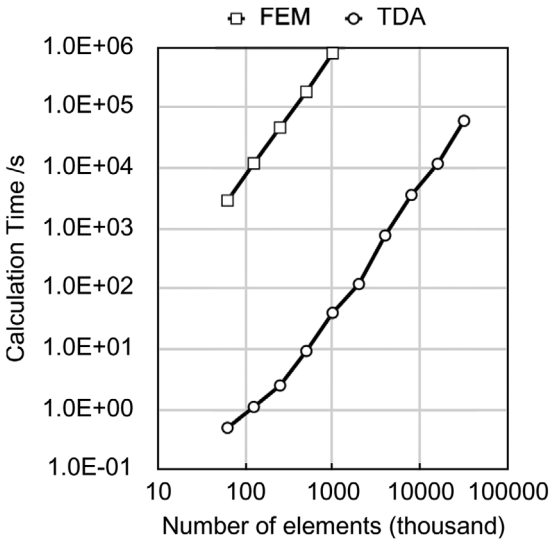

FIGURE 14 Calculation time of FEM and TDA per realization per core with a clock speed of 3.4 GHz

izations were simulated, thereby enabling a direct realization-by-realization comparison between the TDA and FEM3D approaches. The same boundary conditions (Figure 8A) as in the deterministic analyses were adopted.

Table 3 summarizes the random cases analyzed. Two model scales were used, that is, a unit cell with dimensions of 1 m × 1 m × 1 m in the *x*-, *y*-, and *z*-directions, and a more realistic cutoff wall with dimensions of 9 m × 1 m × 10 m. A finer mesh was used for the unit cell verification (Cases VR1 and VR2), and a relatively coarser unit cell verification was used for the larger problem (Case VR3). The same element size was adopted for both the TDA and FEM3D, to minimize the difference caused by mesh size. In each case, 100 realizations were simulated. A typical realization of the unit-cell cutoff wall is shown in Figure 11A and B. The FEM3D and TDA models are almost identical except that the FEM3D model has one less layer. This is because the FEM3D model uses the center coordinates of each element to determine if it is treated, whereas the TDA model uses the nodal coordinates. The three-dimensional view of the treated columns in the unit cell is shown in Figure 11C. Clearly, the gap between the two columns in Figure 11C was successfully captured in Figure 11A and B. As noted for the deterministic analysis, the time to reach the steady-state for the penetrated cutoff wall is considerably less than for the unpenetrated cutoff wall. Hence, in this study, total durations of 1.0×10^5 and 1.0×10^9 s were used for the penetrated and unpenetrated cases, respectively. The normalized time was used to plot both scenarios in the same graph. It is defined as the real time divided by the total duration.

Figure 12A shows the random realizations of discharge rate versus normalized time for Case VR1. Only five realizations are plotted, to clearly distinguish the TDA and FEM3D results, although 100 realizations were calculated in total. Similar to the deterministic analyses, the FEM3D results are slightly lagging behind the TDA results, for the reasons given previously. The discharge rates at three representative normalized timings were extracted, namely, 10%, 20%, and 100%, to make a clear realization-by-realization comparison. The points corresponding to 10% normalized time are largely in a transient state, while those corresponding to 100% are basically at the steady state. A realization-by-realization comparison of the discharge rate estimated by the TDA and FEM3D is plotted in Figure 12B. The results at the initial stage (normalized time = 10%) show that the TDA is consistently 70% higher than the corresponding FEM3D result. This is mainly due to the slight time lag and the high gradient at this timing. Nevertheless, the proportionality between the TDA and FEM3D results is maintained, indicating a strong correlation between the two. The effect of the initial time lag diminishes as the discharge moves toward a steady state. The steady-state results (normalized time = 100%) show that the TDA discharge rate is about 12% greater than the corresponding FEM3D result, which is consistent with Pan et al.[40] Figure 13A shows the results for an average column diameter of 1.2 m (Case VR2), which have a similar trend to those for an average diameter of 0.8 m (Case VR1). However, the former gives a higher ratio of TDA to FEM3D results at 10% normalized time. This may be because, at a larger average diameter, the flow paths are narrower and more tortuous, making them much longer than the thickness of the cutoff wall. This could lead to a larger time-lag between the TDA and FEM3D results. The above results are obtained from single cubic cells. A more realistic comparison was made for a larger model consisting of 10 columns with a length of 10 m. Figure 13B shows that the TDA results for the larger cutoff wall (Case VR3) still match the FEM3D results reasonably well.

TABLE 3 Random verification for the cutoff wall problem

No.	Average diameter of column (m)	Model scale*	Element size** (m)	Element number	Normalized time	Finite element method		TDA		Comparison	
						Mean flow rate (m^3/s)	Calculation duration*** per realization T_{FEM} (s)	Mean flow rate (m^3/s)	Calculation duration per realization T_{TDA} (s)	Ratio of fitting line gradient in Figs. 13 and 14	T_{FEM}/T_{TDA}
VR1	0.8	1 m × 1 m × 1 m	0.02 m × 0.02 m × 0.1 m	25 000	10%	0.81×10^{-6}	528	1.42×10^{-6}	0.17	1.75	3105
					20%	2.59×10^{-6}		3.24×10^{-6}		1.25	
					100%	3.42×10^{-6}		3.86×10^{-6}		1.13	
VR2	1.2	1 m × 1 m × 1 m	0.02 m × 0.02 m × 0.1 m	25 000	10%	1.16×10^{-7}	527	2.40×10^{-7}	0.049	2.06	10 540
					20%	3.76×10^{-7}		4.83×10^{-7}		1.28	
					100%	4.80×10^{-7}		5.39×10^{-7}		1.12	
VR3	1.2	9 m × 1 m × 10 m	0.04 m × 0.04 m × 0.2 m	281 250	10%	1.75×10^{-5}	7.45×10^{4}	3.37×10^{-5}	3.9	1.93	19 103
					20%	5.32×10^{-5}		7.16×10^{-5}		1.34	
					100%	7.45×10^{-5}		8.35×10^{-5}		1.12	

*The model scale refers to the dimensions of the model in *x*-, *y*-, and *z*-directions.

**The element size refers to the dimensions of the element.

***The calculation duration is the calculation time on a single core of central processing unit with a clock speed of 3.4 GHz.

TABLE 4 Convergence study

No.	Horizontal element size* (m)	Vertical element size (m)	Number of columns	Element number	Average calculation time per realization (s)
R1	0.2	0.2	10	22 500	0.12
R2	0.1	0.2	10	90 000	0.70
R3*	**0.04**	**0.2**	**10**	**562 500**	**11.5**
R4	0.02	0.2	10	2250 000	216.7
R5	0.04	2	10	56 250	0.24
R6	0.04	1	10	112 500	0.67
R7	0.04	0.1	10	1125 000	38.5
R8	0.04	0.2	5	250 000	2.93
R9	0.04	0.2	15	875 000	38.1
R10	0.04	0.2	20	1187 500	64.5

*R3 is the reference case.

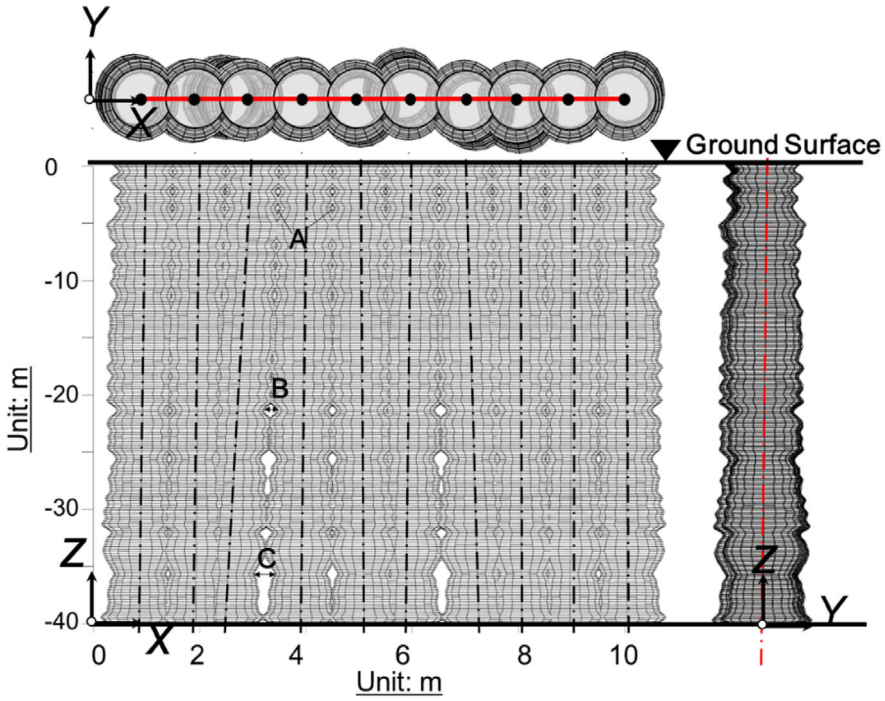

FIGURE 15 A typical realization of a deep cutoff wall (10 columns, center-to-center distance = 1.0 m, overlap = 0.2 m)

3.3 | Calculation expense

Table 3 shows that the average calculation duration per realization using the TDA is only $1/10^3$-$1/10^4$ that of the corresponding FEM3D analysis. This is mainly because, in the three-dimensional FEA, the treated zones consume the majority of the computation cost while contributing little to the resultant discharge rate. In the TDA, the contribution of the treated zones is neglected, and the computation capacity is concentrated on the identified penetrating passages.

A further comparison of calculation expense was made for a cutoff wall with a greater length to explore the full capacity of the TDA. Cutoff walls with a thickness of 1 m, a height of 20 m, and lengths ranging from 1 to 512 m were simulated. The average column diameter was 1.2 m and the center-to-center spacing was 1.0 m, leaving 0.2 m of overlap. The element dimensions in the x-, y-, and z-directions were taken to be 0.04 m × 0.04 m × 0.2 m, so that the total number of elements for the TDA analyses ranged from 62 500 to 32 000 000. For each analysis, the average calculation duration for 20 realizations was calculated to ensure a convergent average time. Preliminary study showed that the calculation expense depends highly

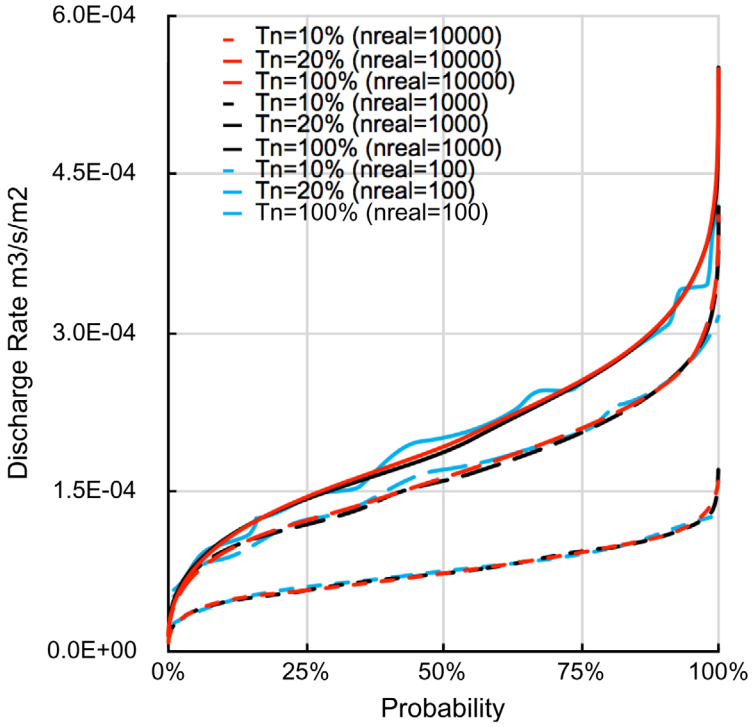

FIGURE 16 Convergence study on the effect of number of realizations (nreal)

on the number of untreated nodes, which varies from realization to realization. Similarly, FEM analyses for the same wall dimensions and element size were performed. Only five realizations were used to evaluate the calculation expense of each FEM analysis because the calculation duration does not vary as significantly as with the TDA. However, due to the huge calculation expense of the FEM, a maximum of 1 000 000 elements were considered, as the calculation of only one realization then took more than 7 days. Figure 14 shows the calculation expense of both approaches. For a typical cutoff wall with dimensions of 20 m × 1 m × 20 m, there are approximately 1 250 000 elements. The calculation duration of one realization for a wall of this size, using the TDA, is less than 1 min. However, the maximum number of elements used with the TDA in this study were around 32 000 000, amounting to a wall length of approximately 500 m, which is consistent with the scale of cutoff walls used in dams. This case takes 32 h for one realization using the TDA, whereas an FEM model at this scale could only be simulated on supercomputers due to the huge demand for memory. However, in reality, it should be possible to analyze a wall with a shorter representative length and then scale up the response to longer problems.[56,57]

4 | CONVERGENCE STUDY

For a problem with specific dimensions and frequency of occurrence of geometric imperfections, it is interesting to do a convergence study to investigate the effect of the number of Monte Carlo simulations, mesh size, and model scale. Intuitively, the mesh size should be proportional to the size of the geometric imperfections (eg, the size of the leaking hole). However, the size of the geometric imperfections may vary significantly from case to case. Hence, it is impractical and unnecessary to identify the smallest geometric imperfections, while the leakages are mainly due to larger ones. On the other hand, one of the main functions of the TDA is to evaluate the probabilistic distribution of discharge rate. As a result, the cumulative distribution curve (for different normalized times) was used to evaluate the adequacy of the mesh in this study. This curve is of engineering interest because it is directly related to performance-based and reliability-based design.[16,17]

Table 4 summarizes various geometrical configurations of a large-scale jet-grouted cutoff wall simulated using the TDA. The reference case (Case R3) consists of 10 columns, each of 20 m in length and 1.2 m in average diameter. The cutoff wall is designed to be installed in a line with an equal spacing of 1 m, so leaving a 200 mm overlap between adjacent columns. Figure 15 shows a typical realization for a similar cutoff wall with a height of 40 m. Clearly, the deviation of the column axis from the vertical accumulates with depth, and this effect is magnified by the diametric variation. At shallower

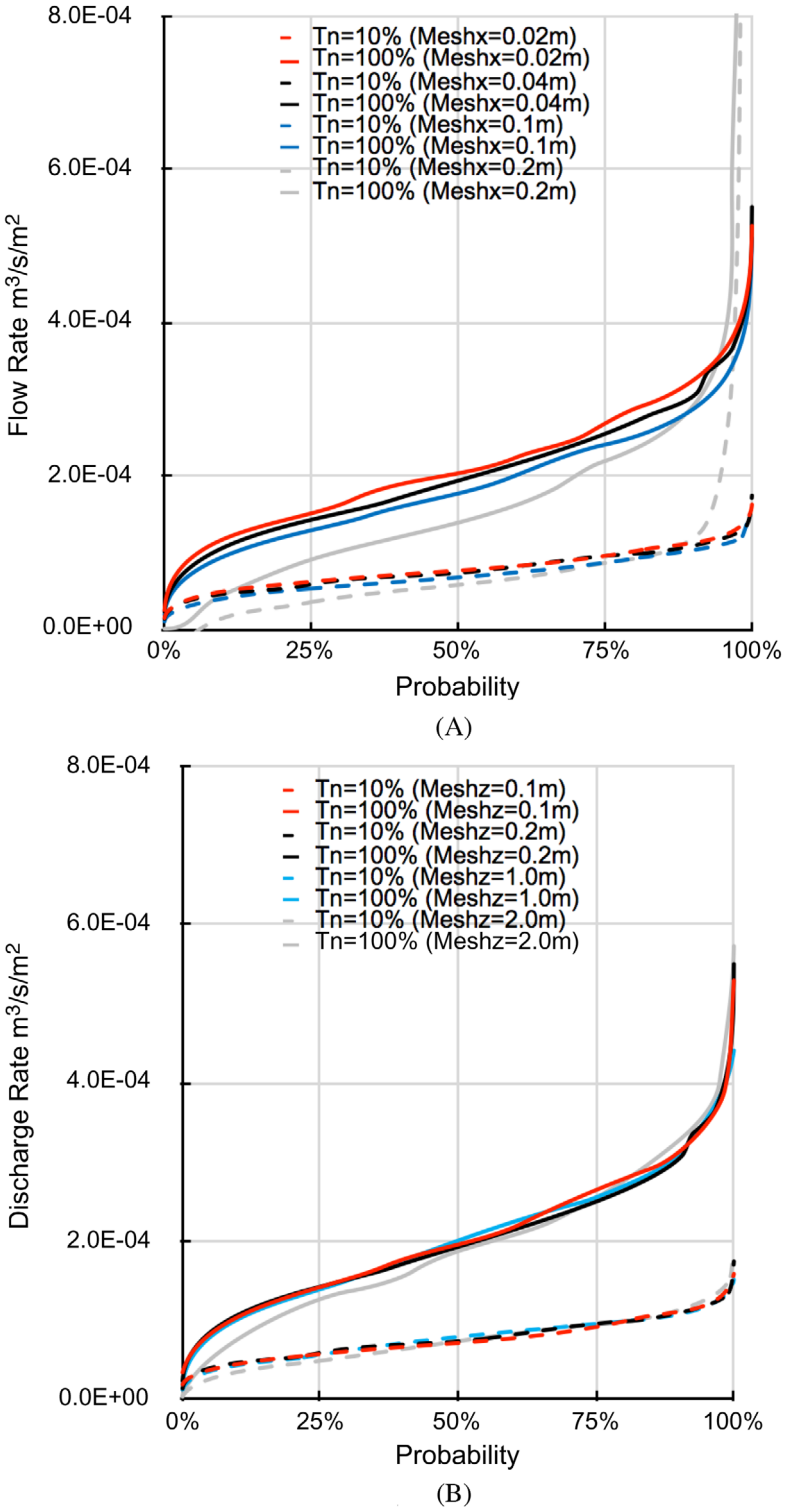

FIGURE 17 Convergence study: (A) effect of horizontal element size on cumulative distribution of discharge rate (x- and y-directions); and (B) effect of vertical element size on cumulative distribution of discharge rate (z-redirection)

depth, the leaking holes (A) are mainly caused by the diametric variation leading to a few small and scattered holes. In contrast, at deeper depths (B and C), they are the result of both axis inclination and diametric variation, resulting in large interconnected leaking holes.

The convergence of the cumulative distribution is important in reliability-based design, as certain fractiles are often used as representative values. Figure 16 shows that 1000 realizations are generally sufficient to achieve a convergent cumulative distribution of the discharge rate, for normalized times of 10%, 20%, and 100%. Figure 17 shows that a horizontal mesh size of 0.04 m and a vertical mesh size of 0.2 m are sufficient to give a convergent result. This is because the size of the geometric

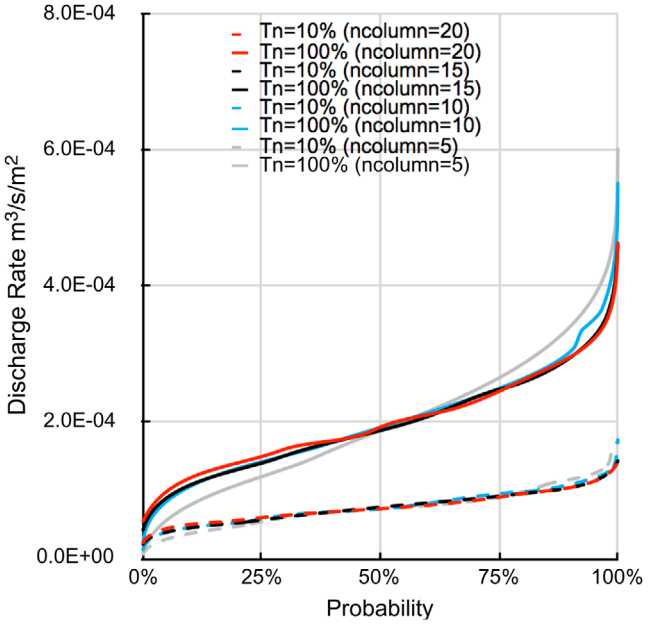

FIGURE 18 Convergence study on the effect of column number on cumulative distribution of discharge rate (the flow rate per unit wall area is the total flow rate normalized by the wall area)

imperfection is generally longer in the vertical direction than in the horizontal direction. All the results are normalized by the area of the wall plane so that the discharge rate with different numbers of columns can be compared. Figure 18 shows that an insufficient number of columns would give a higher discharge rate at high fractiles and a lower discharge rate at low fractiles, indicating a relatively large variation in the result. When 15 columns are used, the cumulative distribution generally converges at high fractiles. In design, the high fractiles are usually used to represent a "rationally pessimistic" scenario.

5 | CONCLUDING REMARKS

A transient-state TDA was proposed to evaluate the discharge rate through geometrically imperfect cutoff walls. By calculating the leakage discharge through the penetrating passages while ignoring the contribution of the treated zone, the TDA can achieve reasonable accuracy at a considerably lower computation cost than the random FEM. Specifically, the discharge rate estimated by the TDA is 1.1-2.0 times the RFEM counterpart, while the former calculation duration is only $1/10^3$-$1/10^4$ that of the latter.

The TDA serves as an efficient and reasonably accurate tool to break down the massive three-dimensional model into relatively few one-dimensional problems. One can use this framework to evaluate other leakage discharges of Laplacian flow through large-scale barriers, because they share similar governing equations. Examples of such flows include leakages during heat conduction and contaminant transport.

ACKNOWLEDGMENTS

This research is supported by the research funding provided by the NRF-NSFC 3rd Joint Research Grant (Earth Science) (Grant No. 41861144022).

ORCID

Yutao Pan https://orcid.org/0000-0001-9504-1347

REFERENCES

1. Sembenelli PG, Sembenelli G. Deep jet-grouted cut-offs in riverine alluvia for Ertan cofferdams. *J Geotech Geoenvir Eng*. 1999;125(2):142-153.
2. Rowe R. Long-term performance of contaminant barrier systems. *Géotechnique*. 2005;55(9):631-678.
3. Croce P, Modoni G. Design of jet-grouting cut-offs. *Proc Inst Civil Eng Ground Improv*. 2007;11(1):11-19.

4. Britton JP, Filz GM, Little JC. The effect of variability in hydraulic conductivity on contaminant transport through soil–bentonite cutoff walls. *J Geotech Geoenvir Eng*. 2005;131(8):951-957.
5. Inazumi S, Ohtsu H, Otake Y, Kimura M, Kamon M. Evaluation of environmental feasibility of steel pipe sheet pile cutoff wall at coastal landfill sites. *J Mat Cyc Was Manag*. 2009;11(1):55-64.
6. Zhan L, Liu W, Zeng X. Parametric study on breakthrough time of vertical cutoff wall for MSW landfills and simplified design formula for wall thickness. *Chin J Geotech Eng*. 2013;35(11):1988-1996.
7. Koda E, Osinski P. Bentonite cut-off walls: solution for landfill remedial works. *Environ Geotech*. 2016;4(4):223-232.
8. Wang Z-F, Shen S-L, Ho C-E, Kim Y-H. Investigation of field-installation effects of horizontal twin-jet grouting in Shanghai soft soil deposits. *Can Geotech J*. 2013;50(3):288-297.
9. Takai A, Inui T, Katsumi T. Evaluating the hydraulic barrier performance of soil-bentonite cutoff walls using the piezocone penetration test. *Soil Found*. 2016;56(2):277-290.
10. Brown AJ, Bruggemann DA. Arminou Dam, Cyprus, and construction joints in diaphragm cut-off walls. *Géotechnique*. 2002;52(1): 3-13.
11. Van Tol AF, Veenbergen V, Maertens J. *Diaphragm Walls, A Reliable Solution for Deep Excavations in Urban Areas*. London: Deep Foundation Institute, DFI and EFFC; 2010:335-342.
12. Spruit R, van Tol AF, Broere W, Slob E, Niederleithinger E. Detection of anomalies in diaphragm walls with crosshole sonic logging. *Can Geotech J*. 2014;51(4):369-380.
13. Spruit R, Van Tol AF, Broere W, Slob E. Detecting anomalies in diaphragm walls with electrical resistance measurements. *Near Surf Geophy*. 2016;14(6):481-491.
14. Hong CS, Shackelford CD. Mixed metals migration through zeolite-amended backfills for vertical cut-off walls. *Environ Geotech*. 2017;6(4):225-241.
15. Wang Y, Chen Y, Xie H, Zhang C, Zhan L. Lead adsorption and transport in loess-amended soil-bentonite cut-off wall. *Eng Geol*. 2016;215:69-80.
16. Pan Y, Liu Y, Hu J, Sun M, Wang W. Probabilistic investigations on the watertightness of jet-grouted ground considering geometric imperfections in diameter and position. *Can Geotech J*. 2017;54(10):1447-1459.
17. Pan Y, Liu Y, Chen E. Probabilistic investigation on defective jet-grouted cut-off wall with random geometric imperfections. *Géotechnique*. 2019;69(5):420-433.
18. Morey J, Campo DW. Quality control of jet grouting on the Cairo metro. *Proc Inst Civil Eng Ground Improv*. 1999;3(2):67-75.
19. Ni J, Cheng W-C. Characterising the failure pattern of a station box of Taipei Rapid Transit System (TRTS) and its rehabilitation. *Tunn Undergr Sp Tech*. 2012;32:260-272.
20. Pujades E, Carrera J, Vázquez-Suñé E, Jurado A, Vilarrasa V, Mascuñano-Salvador E. Hydraulic characterization of diaphragm walls for cut and cover tunnelling. *Eng Geol*. 2012;125:1-10.
21. Shen S-L, Wang Z-F, Yang J, Ho C-E. Generalized approach for prediction of jet grout column diameter. *J Geotech Geoenvir Eng*. 2013;139(12):2060-2069.
22. Wu Y-X, Shen S-L, Xu Y-S, Yin Z-Y. Characteristics of groundwater seepage with cut-off wall in gravel aquifer. I: Field observations. *Can Geotech J*. 2015;52(10):1526-1538.
23. Wu Y-X, Shen S-L, Yin Z-Y, Xu Y-S. Characteristics of groundwater seepage with cut-off wall in gravel aquifer. II: Numerical analysis. *Can Geotech J*. 2015;52(10):1539-1549.
24. Tan Y, Lu Y. Forensic diagnosis of a leaking accident during excavation. *J Perf Const Facil*. 2017;31(5):04017061.
25. Li L-P, Chen D-Y, Li S-C, Shi S-S, Zhang M-G, Liu H-L. Numerical analysis and fluid-solid coupling model test of filling-type fracture water inrush and mud gush. *Geomech Eng*. 2017;13(6):1011-1025.
26. Wang J, Liu X, Wu Y, et al. Field experiment and numerical simulation of coupling non-Darcy flow caused by curtain and pumping well in foundation pit dewatering. *J Hydrol*. 2017;549:277-293.
27. Castaldo P, Jalayer F, Palazzo B. Probabilistic assessment of groundwater leakage in diaphragm wall joints for deep excavations. *Tunn Undergr Sp Tech*. 2018;71:531-543.
28. Lacombe S, Sudicky E, Frape SK, Unger AJA. Influence of leaky boreholes on cross-formational groundwater flow and contaminant transport. *Wat Resour Res*. 1995;31(8):1871-1882.
29. Texplor. *Microgravity Report Underground Investigation*. Naples; 2013.
30. Van Tol A. Schadegevallen bij bouwputten. [Damage caused by deep excavations]. *Cement*. 2007;59(6):6-13.
31. Fenton GA, Griffiths DV. *Flow Through Earth Dams with Spatially Random Permeability*. Colorado School of Mines, Geomechanics Research Center; 1994.
32. Griffiths DV, Fenton GA. Probabilistic analysis of exit gradients due to steady seepage. *J Geotech Geoenvir Eng*. 1998;124(9):789-797.
33. Srivastava A, Babu GS, Haldar S. Influence of spatial variability of permeability property on steady state seepage flow and slope stability analysis. *Eng Geol*. 2010;110(3-4):93-101.
34. Drakos S, Pande G. Stochastic finite element analysis for transport phenomena in geomechanics using polynomial chaos. *Glob J Res Eng*. 2015;15(2).
35. Fenton GA, Liza R, Lake CB, Menzies WT, Griffiths DV. Statistical sample size for quality control programs of cement-based "solidification/stabilization". *Can Geotech J*. 2015;52(10):1620-1628.

36. Van Esch J, Van Tol AF, Havinga H, Duijvestijn A, Schat B, de Wit J. Functional analyses of jetgrout bodies based on Monte Carlo simulations. 11th International Conference on Computer Methods and Advances in Geomechanics. Torino, Italy; 2005.
37. Van Tol AF, Koster S, Ramier JG, Verruijt A, Vrijing J. Imperfections in jetgrout layers. International Conference on Soil Mechanics and Geotechnical Engineering. 2001.
38. Wu Y-X, Shen S-L, Lyu H-M, Zhou A. Analyses of leakage effect of waterproof curtain during excavation dewatering, *J Hydrol*. 2020;583:124582.
39. Wu H-N, Shen S-L, Chen R-P, Zhou A. Three-dimensional numerical modelling on localised leakage in segmental lining of shield tunnels. *Comp Geotech*. 2020;122:103549.
40. Pan Y, Yi J, Goh S-H, Hu J, Wang W, Liu Y. A three-dimensional algorithm for estimating water-tightness of cement-treated ground with geometric imperfections. *Comp Geotech*. 2019;115:103176.
41. Malusis MA, Maneval JE, Barben EJ, Shackelford CD, Daniels ER. Influence of adsorption on phenol transport through soil–bentonite vertical barriers amended with activated carbon. *J Contam Hydrol*. 2010;116(1-4):58-72.
42. Bruce DA, DePaoli B, Mascardi C, Mongilardi E. Monitoring and quality control of a 100 meter deep diaphragm wall. *DFI International Conference on Piling and Deep Foundations*. London; 1989:15-18.
43. Modoni G, Flora A, Lirer S, Ochmański M, Croce P. Design of jet grouted excavation bottom plugs. *J Geotech Geoenvir Eng*. 2016;142(7):04016018.
44. Amos PD, Bruce DA, Lucchi M, Watkins N, Wharmby N. Design and construction of deep secant pile seepage cut-off walls under the Arapuni Dam in New Zealand. *USSD 2008 Conference*. Portland, OR; 2008.
45. Pan Y, Fu Y. Effect of random geometric imperfections on the water-tightness of diaphragm wall. *J Hydr*. 2020;580:124252.
46. Arroyo M, Gens A, Croce P, Modoni G. Design of jet-grouting for tunnel waterproofing. Proceedings of the 7th International Symposium on the Geotechnical Aspects of Underground Construction in Soft Ground: TC28-IS. Rome: London, United Kingdom: Taylor & Francis Group; 2012.
47. Liu Y, Lee F-H, Quek S-T, Chen E, Yi J-T. Effect of spatial variation of strength and modulus on the lateral compression response of cement-admixed clay slab. *Géotechnique*. 2015;65(10):851-865.
48. Liu Y, Pan Y, Sun M, Hu J, Yao K. Lateral compression response of overlapping jet-grout columns with geometric imperfections in radius and position. *Can Geotech J*. 2018;55(9):1282-1294.
49. Pan Y, Liu Y, Lee FH, Phoon KK. Analysis of cement-treated soil slab for deep excavation support—a rational approach. *Géotechnique*. 2019;69(10):888-905.
50. Phoon K-K, Kulhawy FH. Characterization of geotechnical variability. *Can Geotech J*. 1999;36(4):612-624.
51. Hicks MA, Samy K. Influence of heterogeneity on undrained clay slope stability. *Quart J Eng Geol Hydrogeol*. 2002;35(1):41-49.
52. Zhu H, Zhang L. Characterizing geotechnical anisotropic spatial variations using random field theory. *Can Geotech J*. 2013;50(7):723-734.
53. Chew S, Kamruzzaman A, Lee F. Physicochemical and engineering behavior of cement treated clays. *J Geotech Geoenvir Eng*. 2004;130(7):696-706.
54. Bear J, Verruijt A. *Modeling Groundwater Flow and Pollution*. Vol. 2. Springer Science & Business Media; 2012.
55. Schirén W. *Finite Element Method for 1D Transient Convective Heat Transfer Problems* [Bachelor Thesis]. Småland, Sweden: Linnaeus University; 2018.
56. Hicks MA, Li Y. Influence of length effect on embankment slope reliability in 3D. *Int J Numer Anal Method Geomech*. 2018;42(7):891-915.
57. Hicks MA, Spencer WA. Influence of heterogeneity on the reliability and failure of a long 3D slope. *Comp Geotech*. 2010;37(7-8):948-955.
58. Croce P, Flora A, Modoni G. *Jet Grouting: Tecnica, Progetto E Controllo*. Hevelius; 2004.
59. Langhorst OS, Schat BJ, de Wit JCWM, et al. Design and validation of jet grouting for the Amsterdam Central Station. Geotechniek, Special Number on Madrid XIV European Conference of Soil Mechanics and Foundation Engineering. 2007.
60. Eramo N, Modoni G, Arroyo M. Design control and monitoring of a jet grouted excavation bottom plug. Proceedings of the 7th International Symposium on the Geotechnical Aspects of Underground Construction in Soft Ground. London: Taylor & Francis Group; 2012.

How to cite this article: Pan Y, Hicks MA, Broere W. An efficient transient-state algorithm for evaluation of leakage through defective cutoff walls. *Int J Numer Anal Methods Geomech*. 2021;45:108–131. https://doi.org/10.1002/nag.3145